Int. Journ. of Fracture 22 (1983) 15–39

Comparison of finite element solutions with analytical and experimental data for elastic-plastic cracked problems

M.H. BLEACKLEY and A.R. LUXMOORE

Department of Civil Engineering, University College, Swansea, West Glamorgan, SA2 8PP, UK

(Received May 21, 1981; in revised form December 15, 1981)

ABSTRACT

Non-linear finite element results from a round robin are compared with empirical and experimental data obtained for three types of geometries: compact specimen, three-point bend specimen and a center-cracked panel subject to uniaxial loading. The solution parameters to be compared in various forms are: applied load, clip gauge displacement, Rice J-integral (with no limit placed on method of calculation), K_I, crack opening profiles and plastic zone development.

1. Introduction

Numerical methods of stress analysis are powerful tools which can produce solutions for elastic-plastic deformation of solids and in this connection have found widespread use in fracture mechanics. Unfortunately, the absence of exact solutions creates difficulties in assessing the accuracy of these solutions. A previous comparison [1] has shown the serious discrepancies that can exist between solutions to an identical problem, even for programs based on similar formulations.

As well as checking for self-consistency amongst different solutions of the same problem, it is also useful to check numerical results with actual experimental results. The suggested round robin problems have all been tested experimentally, and hence loads and displacements can be compared directly.

This paper summarises the results of a round robin problem given at the Second International Conference on Numerical Methods in Fracture Mechanics, held at University College Swansea, U.K., in July, 1980. For this conference the following problems were suggested:

(1) Elastic-plastic compact specimen (CS) analysis.
(2) Elastic-plastic three-point bend (BEND3) analysis.
(3) K_I calculations for BEND3 and single edge notch tension (SENT) specimens.
(4) Slow crack growth of a center-cracked panel (CCP) subject to uniaxial tension.

A brief account of the program together with procedures used was requested from each participant. The results presented at the conference were in an anonymous form, with each contributor designated by a letter of the alphabet.

2. Description of the problems

The specimens chosen may be represented by two-dimensional numerical models. The BEND3 specimen can be considered as a plane strain problem, whilst the CS and CCP

geometries are represented by plane stress. These two extremes represent the overall deformation behaviour of the specimens.

The CS and BEND3 specimens involve static analysis only, and no fracture loads are quoted. In the CCP specimen, stable crack growth was monotored, and accurate modelling of this specimen requires the use of some appropriate fracture criterion, in addition to the elastic-plastic analysis.

The four problems presented involve a considerable amount of computing effort, and participants were not obliged to carry out all the computations. Partial results for any particular specimen were acceptable.

No limitation is placed on the method of calculating the J-integral. Table 1 gives some of the definitions of J used in this paper.

TABLE 1
Summary of definitions for evaluating the J-integral

J_{co}	Contour integral [3]	$J_{co} = \int_{\Gamma}\left(w\,dy - T_i\frac{du_i}{dx}ds\right)$
J_{pe}	Difference in potential energy [4]	$J_{pe} = -\frac{1}{B}\frac{dU}{da}$
J_{vi}	Virtual crack extension [5]	
J_{es}	Sumpter's energy split [6]	$J_{es} = \frac{1}{B(W-a)}(\eta_e\,dUe + \eta_p\,dUp)$

J_{co} is usually averaged over a number of paths to render J_{co}. Two load/displacement curves (and hence two computer runs) are required to calculate J_{pe} from two equivalent geometries with their respective crack lengths differing by da. dU is the difference in energy absorbed by the two geometries (or the difference in area under the two load/displacement curves).

For J_{vi}, a solution for one single crack length is required and the crack is advanced by moving nodal points rather than removing nodal tractions at the crack tip. Thus the change in structural stiffness can be calculated, enabling dU/da to be obtained.

J_{es} requires one computer run to obtain the elastic (U_e) and plastic (U_p) absorbed energy components.

2.1. *Compact specimen (CS)*

In an experimental investigation on thickness effects at the Institut für Eisenhüttenkunde, in Aachen, W. Germany, standard CS specimens of varying thickness were tested. For the thinnest specimen, 3 mm thick, considerable plasticity occurred prior to unstable fracture. This specimen has been chosen as the numerical model. Load and clip gauge displacements were monitored during testing, with the clip gauge measuring the displacements at the load line between the points marked A and B on the machined notch in Fig. 1. Whether to model the loading pin hole was left to the contributors themselves.

The material properties are quoted in Fig. 2. Two results were required for this specimen, the load and J-integral versus clip gauge displacment. The specimen was loaded experimentally by load control, with the experimental value of J obtained from the load/displacement curve using Merkle and Corten's equation in Ref. [2].

A list of persons responsible for the nine contributions is shown in Table 2.

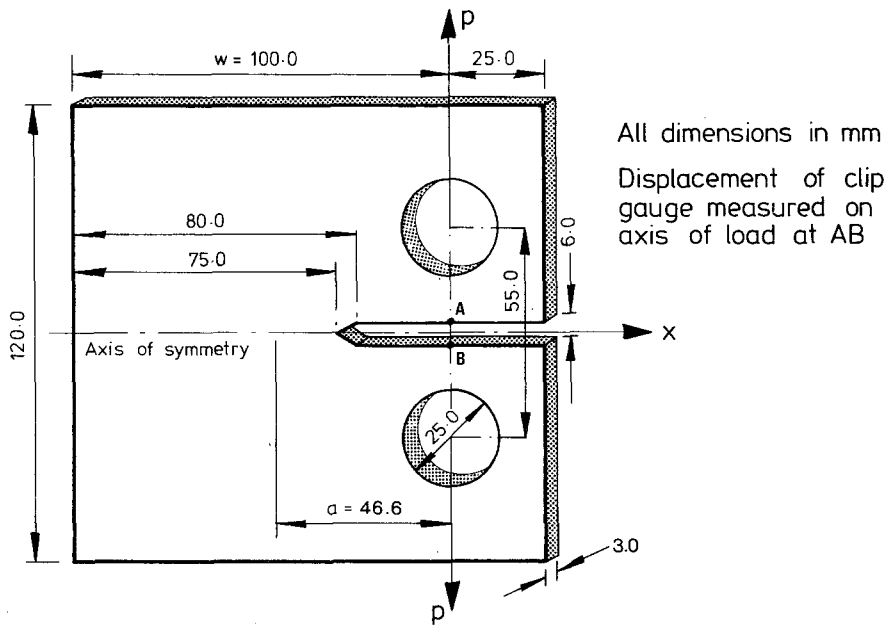

Figure 1. Geometry of compact tension specimen.

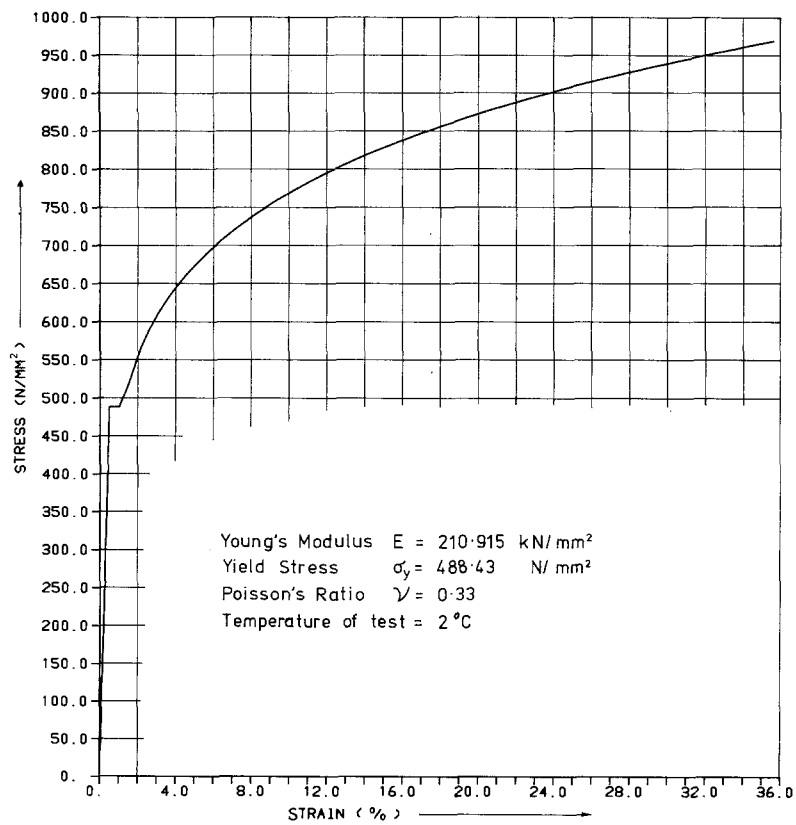

Figure 2. Stress-strain curve for steel ST E 47 pertaining to the compact tension specimen.

TABLE 2
Participants in the compact specimen round robin problem

M. Bleackley	University College of Swansea, West Glamorgan, Wales, U.K.
T.K. Hellen	Central Electricity Generating Board, Berkeley Nuclear Laboratories, Gloucestershire, England.
K. Kashima	Central Research Institute of Electrical Power, Japan.
D. Mackay	University College of Swansea, West Glamorgan, Wales, U.K.
M. Rahimian and Ehrlacher	Laboratoire de Mecanique des Solides, Ecole Polytechnique, palaiseau, France.
M. Sakata, S. Aoki and K. Kishimoto	Tokyo Institute of Technology, Japan.
T. Watanabe	Century Research Center Corporation, Japan.
G. Yagawa, T. Aizawa and Y. Takahashi	University of Tokyo, Japan.
Y. Yamada and I. Nishiguchi	University of Tokyo, Japan.

2.2. *Three-point bend* (BEND3) *specimen*

A major problem in fracture mechanics is posed by the presence of cracks in welds. In a recent experimental investigation (Dawes, 1976, unpublished), a substantial difference in fracture behaviour was observed between shallow and deep cracks in welded specimens tested in a three-point bend configuration, Fig. 3, with deep cracks producing brittle behaviour.

The specimen shown in Fig. 3 was modelled with a/W ratios of 0.1, 0.15 and the standard 0.5 [7], using the material properties quoted in Fig. 4. In the experimental tests only clip gauge displacements were monitored with the clip gauge points located at A, Fig. 3. The gauge measured displacements 3 mm above the top surface of the specimen.

Five sets of results were required from this specimen:

(a) Load versus clip gauge displacement.
(b) J versus clip gauge displacement.
(c) Crack opening profiles for $a/W = 0.5$ at a clip gauge displacement of 0.7 mm.
(d) Center of rotation r.
(e) Plastic zone profile for $a/W = 0.5$ at a clip gauge displacement of 0.7 mm.

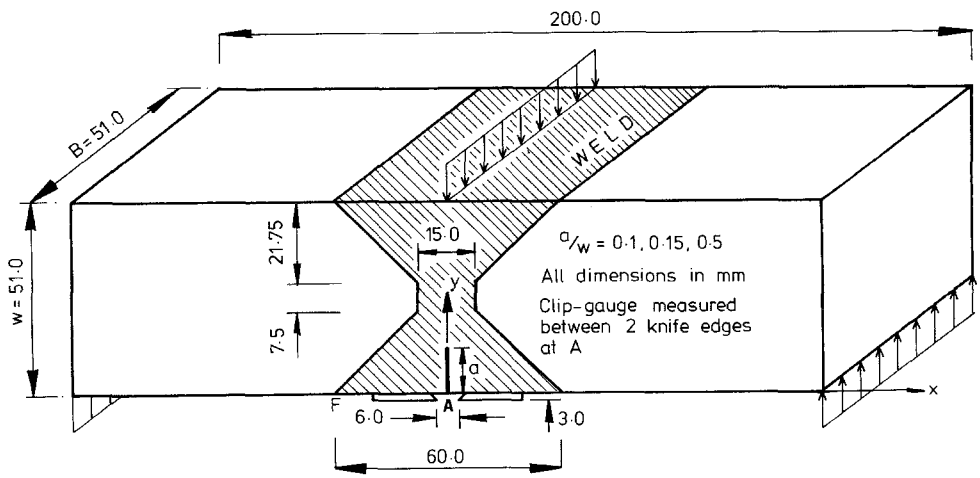

Figure 3. Geometry of the three point BEND specimen.

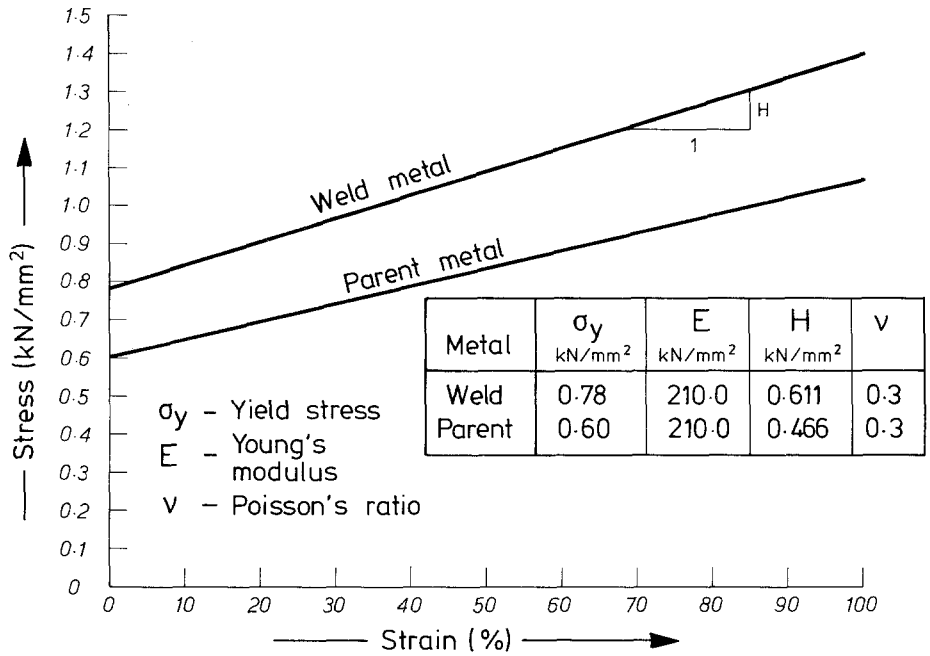

Figure 4. Stress-strain curves for the weld and parent metal of the three point BEND specimen.

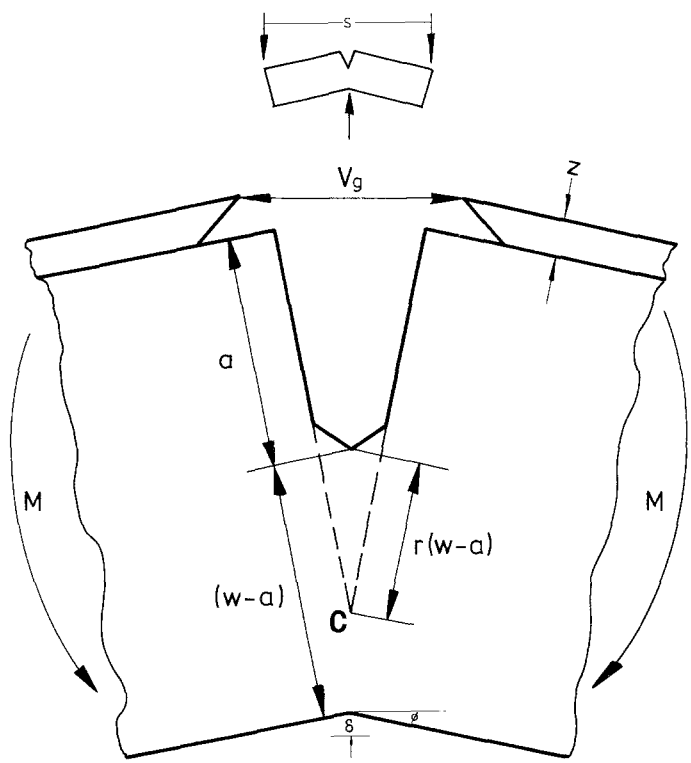

Figure 5. Relationship between V_g and r for a rigid rotation about C.

The center of rotation is important when converting clip gauge displacement to crack tip displacement (Fig. 5). The center of rotation is measured by the distance from the crack tip, and this distance is put into non-dimensional form by dividing by the ligament length $(W - a)$ giving the ratio r.

The extent of the plastic zone, as calculated numerically, is very sensitive to the numerical refinements used. Although the plastic zones were not observed experimentally, it is of considerable interest to compare the different numerical evaluations, especially in a problem involving a boundary between dissimilar materials.

The specimens were loaded experimentally by load control and from the load/load-point displacement curve experimental J_{es} values were obtained.

A list of contributors is shown in Table 3.

TABLE 3
Participants in the three-point bend weld round robin problem

M. Bleackley	University College of Swansea, West Glamorgan, Wales, U.K.
K. Kashima	Central Research Institute of Electrical Power, Japan.
M. Kikuchi	Tokyo Science University, Japan.
N. Mukaimachi	J.G.C. Corporation, Japan.
T. Murakami and T. Mori	Toshiba Electric Comapany, Japan.
T. Watanabe	Century Research Center Corporation, Japan.

A similar analytical round robin for a three-point bend homogeneous specimen with $a/W = 0.5$ has been carried out by Wilson and Osias [1].

2.3. K_I *Stress intensity factors for the* BEND3 *and* SENT *geometries*

It is now well extablished that numerical methods can calculate stress intensity factors with a high order of accuracy. The main interest has now centred on the cost effectiveness of varying solutions. Reducing the number of degrees of freedom will reduce the cost, but it will also reduce the accuracy. Hence special crack tip formulations and other tehcniques have been devised to overcome this problem.

Using the geometry of Fig. 3 with a/W values of 0.10 and 0.50 and the elastic properties in Fig. 4, K_I values are required for the BEND3 geometry in Fig. 3, together with the same specimen loaded in tension by uniform displacements across the end faces. These calculations are repeated for a weld material having a Young's modules of 170.0 kN/mm^2. These K_I values are quoted in the dimensionless form $F_I = K_I B\sqrt{W}/P$, where P is the load.

The assessment of cost effectiveness is not simple because the same program run on two different computers can produce quite different costings. However as cost is the main measure of effectiveness, participants were asked to quote the cost in dollars for their K_I calculations.

A list of contributors is shown in Table 4.

TABLE 4
Participants in the nondimensional stress intensity factor round robin problem

P. Bartholomew	Royal Aircraft Establishment, Farnborough, U.K.
M. Bleackley	University College of Swansea, West Glamorgan, Wales, U.K.
T. Watanbe and G. Yagawa	Century Research Center Corporation; University of Tokyo, Japan.
G. Yagawa and H. Hirayama	University of Tokyo, Japan.
G. Yagawa and Y. Takahashi	University of Tokyo, Japan.

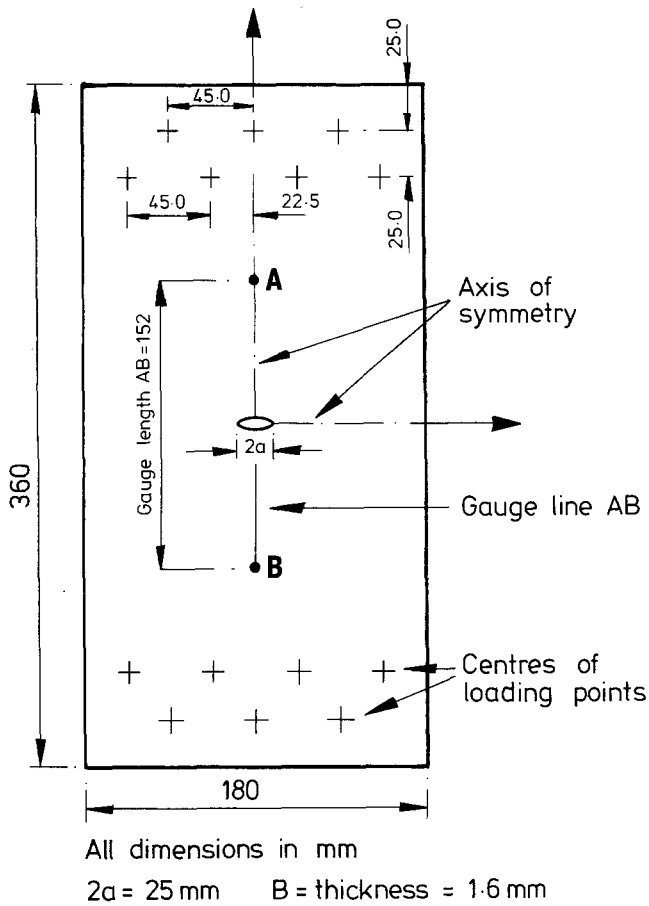

Figure 6. Geometry of the aluminium alloy centre notch.

2.4. *Center-cracked panel* (CCP)

In an *R*-curve study [8] on the fracture behavior of high strength aluminium thin plates 1.6 mm thick center-cracked panels (Fig. 6) were clamped either end by rigid steel bars. These steel bars were bolted through the holes indicated and loaded in a stiff loading machine, hence simulating the application of constant displacement across the two ends of the specimen. During the loading sequence, stable crack growth was observed, i.e. increasing crack length under increasing load up to a maximum load. After this point cracking became increasingly unstable.

The initial crack plane was perpendicular to the loading axis. During the first 1–2 mm of stable crack growth, the crack plane rotated through approximately 45 degrees, and all subsequent crack growth was of this slanting type. Significant amounts of plasticity occurred during the loading cycle.

The specimen displacement was measured between the gauge points *AB*, 152 mm apart. The material properties and crack extensions are given in Fig. 7. A load versus gauge-point displacement for the specimen was required. To obtain this, an appropriate fracture criterion in conjunction with the numerical analysis is required.

A list of contributors is shown in Table 5.

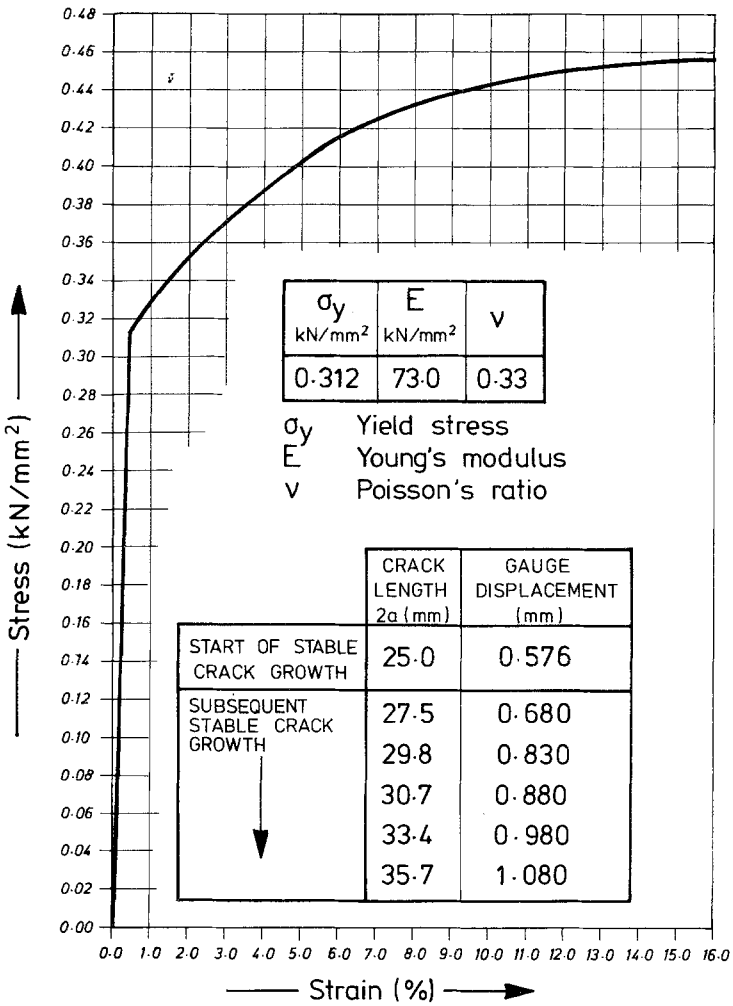

Figure 7. Piecewise stress-strain curves for the aluminium alloy centre notch specimen.

TABLE 5
Participants in the center-cracked panel round robin

M. Bleackley	University College of Swansea, West Glamorgan, Wales, U.K.
T. Takahashi, T. Aizawa and G. Yagawa	University of Tokyo, Japan.
Y. Yamada and I. Nishiguchi	Institute of Industrial Science, University of Tokyo.

3. Results

3.1. *Compact specimen results*

The numerical details of the nine contributors (A–I) are listed in Table 6. The results are plotted as 1) the applied load (P)/clip gauge displacement (V_g), Fig. 8 and 2) J/V_g results Fig. 9. Four contributors chose the initial stiffness and the remaining five the tangential stiffness method of solving the non-linearities of the problem. Small strain incremental plasticity theory was employed by eight of the contributors, while the ninth (G) employed a large rotation (updated Lagrangian) formulation.

TABLE 6
Basic details of the compact tension specimen round robin problem

Solution	Plasticity method	Element type	Number of elements in half space mesh	Number of degrees of freedom	Calculation method of J integral	Hole modelled	Comments
A	Tangential stiffness	8 node Isoparametric	52	400	Path integral (Mean of 4 paths)	Yes	Applied load
B	Tangential stiffness	4–8 noded Isoparametric	62	316	Path integral (Mean of 6 paths)	Yes	Deformation theory
C	Initial stiffness	8 node Isoparametric	71	522	Virtual crack estension	Yes	
D	Tangential stiffness	3 node Constant strain triangle	607	698	Path integral (Mean of 5 paths)	Yes	
E	Tangential stiffness	3 node Constant strain triangle	392	458	Path integral (Mean of 15 paths)	Yes	
F	Initial stiffness	8 node Isoparametric	84	566	Path integral (Mean of 9 paths)	No	
			100	670	–	No	Applied displacement Disp. formulation
			150	982	–	No	
G	Tangential stiffness	8 node Isoparametric	84	566	Difference in potential energy $\Delta a = 0.5, 1.0$ mm	No	Small strain, large rotation formulation
H	Initial stiffness	4 and 6 noded Isoparametric	339	572	Path integral (1 path calculated)	Yes	
I	Initial stiffness	8 and 6 noded Isoparametric	60	436	Path integral (Typical path chosen)	Yes	$1/\sqrt{r}$ singularity elements around crack tip

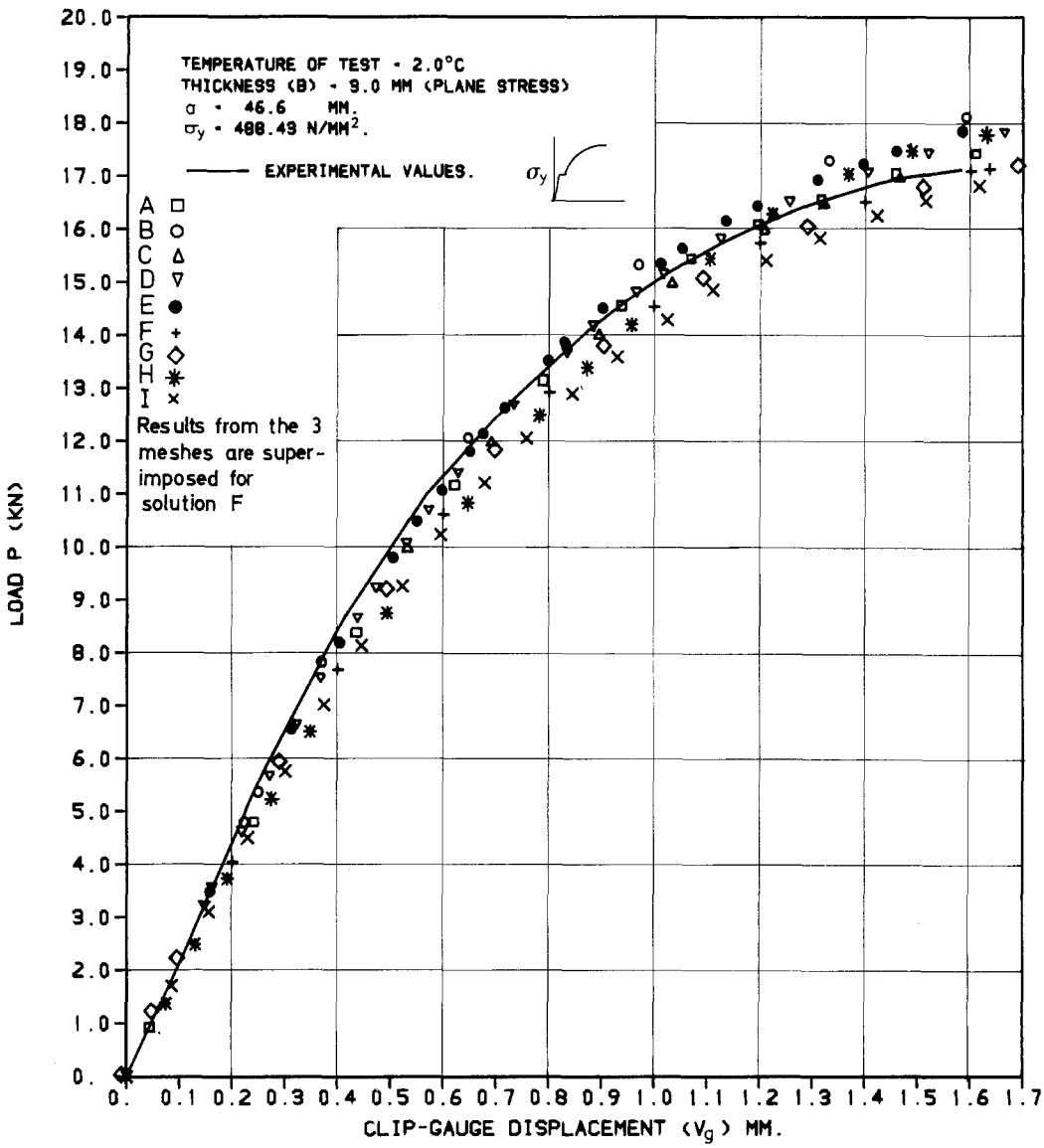

Figure 8. *Round robin.* Variation of load with clip gauge displacement (V_g) for the 3 mm thick compact tension specimen.

Due to symmetry only one half of the specimen was analyzed. Ten separate meshes were used as contributor F modelled the problem with three different meshes, and solution G used the coarsest of these latter three meshes. Four of the contributors chose eight-noded isoparametric elements, two constant-strain triangular elements and the remaining three a mixture of isoparametric elements. Of these three latter contributors, H and I utilized the six-noded triangle and parabolic elements and B used various combinations of four- to eight-noded elements. In addition contributor I used $1/\sqrt{r}$ singularity crack tip elements [9]. Only the meshes used by contributor F and G did not model the loading pin hole.

Seven of the contributors modelled the specimen by applied load and two by applied displacements. Eight contributors obtained one solution each for J. Seven contributors chose to calculate J by $\bar{J}_{co}$ and one by J_{vi}. The ninth contributor (G) obtained three solutions using J_{pe} with: 1) $da = 0.5$ mm using a one node release, 2) $da = 0.5$ mm using a two node release

and 3) $da = 1.0$ mm using a two node release. For the contour method, $\bar{J}_{co}$ was averaged over a number of paths except solution H which was calculated from only one path and solution I where a typical path was chosen that gave a good representation of the other path values. For the eleven P/V_g results each set of participants contributed one solution except case F which contributed three.

There is good agreement between the experimental and numerical load/displacement curves in Fig. 8 although element type, mesh pattern and plasticity method vary with solution. At low load levels the numerical and experimental values coincide but at the higher load levels the experimental values are interspersed between the numerical ones. For case F's three solutions threre is no discernible difference between solutions even though there is a widely varying number of elements (although the meshes have the same pattern) between the finest and coarsest mesh.

The J/V_g curves of Fig. 9 are in very good agreement for all solutions except cases H and one solution from case G. The poor representation of contributor H may be attributable to $\bar{J}_{co}$ being obtained from a single contour and not an average. One of G's three solutions for J_{pc} is not in good agreement with the general body of results for $da = 0.5$ mm using a one node release. For a two node release as with one other of G's solutions, the crack length is extended by da over one element side, as a parabolic element is used. For a one node release, da is taken over just half an element side, so that the crack tip is at the mid-side node. As the crack opens, deformation occurs between the two remaining restrained nodes situated at and immediately behind the crack tip. This is because the element deforms in a parabolic fashion and cannot accommodate a straight boundary behind the crack tip. This gives rise to a small but appreciable increase in the limit load over the corresponding value for $da = 0.5$ mm using a two node release. Hence there is a smaller change in potential energy dU and so a reduction in J_{pc}.

Shiratori and Miyoshi [10] have reported a similar round robin analysis of a compact specimen conducted in Japan. They divided the analysis into a "standard" problem where both the mesh and J_{co} paths were specified by the organizers, and a "non-standard" problem where no limits were imposed. The agreement between different solutions for the standard problem was extremely good, and understandably better than for their non-standard case. The agreement reported in this paper lies somewhere between these two Japanese comparisons.

3.2. *Three-point bend specimen results*

The six contributions (J–O) for this geometry presented ten solutions (Table 7). Six of the solutions were for $a/W = 0.5$, and two each for $a/W = 0.1$ and $a/W = 0.15$. Of the six contributions, four were obtained using tangential stiffness and the remaining two by initial stiffness. Small strain incremental theory was employed in all the contributions.

Due to symmetry only one half of the specimen was analyzed, with the elements arranged so as to accommodate the weld. Eight different meshes were constructed for the ten solutions, to model the required different crack lengths, one each for J, L, M, N and two for K, O. Four contributors chose eight-noded isoparametric elements and the remaining two constant-strain triangles.

With the exception of solution O, which used applied displacements, the solutions were obtained using applied force increments. Four of the contributors obtained J from J_{co} and two by virtual crack extension (J_{vi}).

Figures 10a, b, c show the load/clip gauge displacement (V_g^*) curves for $a/W = 0.1, 0.15$

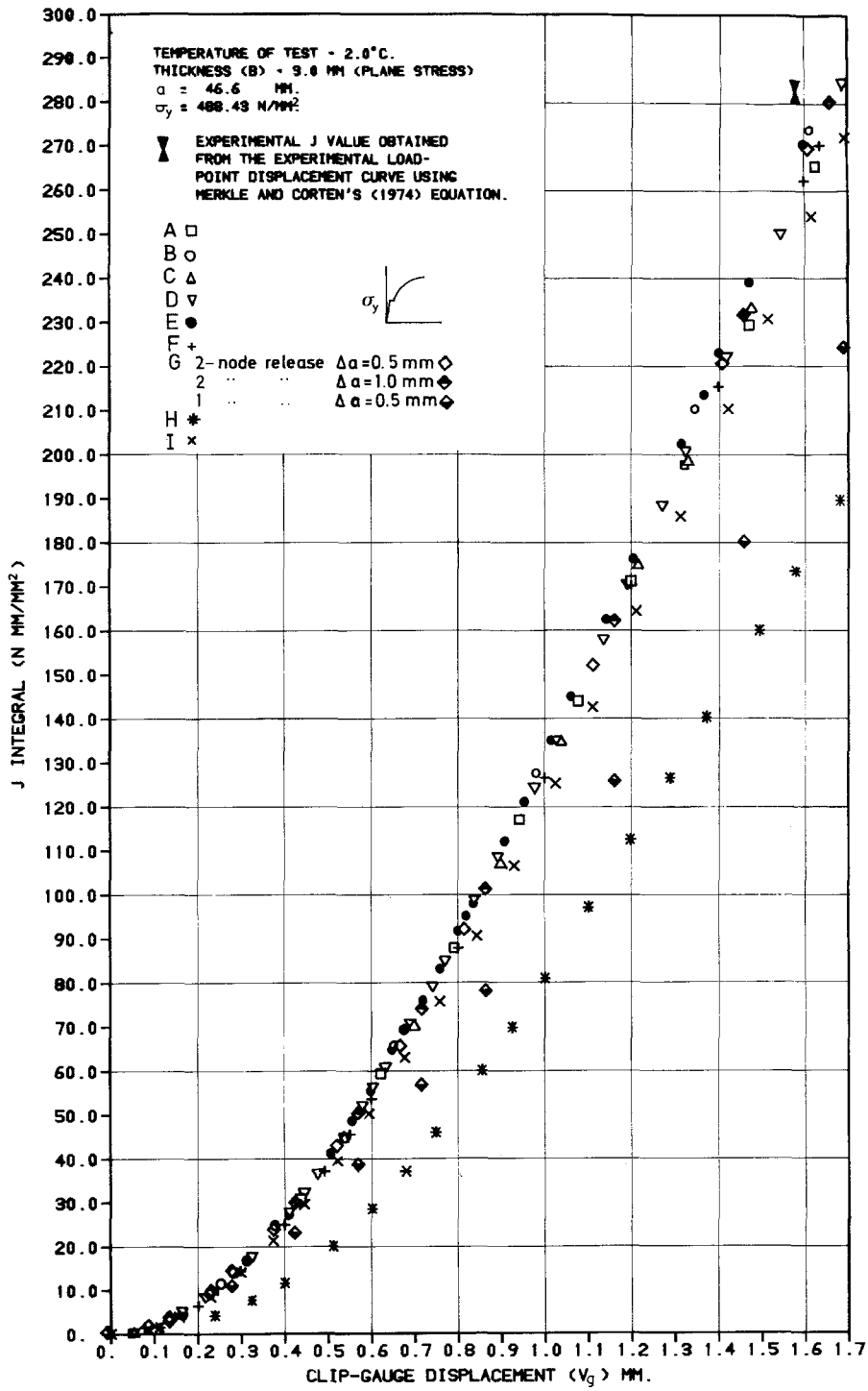

Figure 9. *Round robin.* Variation of the J integral with clip gauge displacement (V_g) for the 3 mm thick compact tension specimen.

TABLE 7
Basic details of the three point bend weld specimen round robin problem

Solution	Plasticity method	Element type	Calculation method of J integral	a/w	Number of elements in half space mesh	Number of degrees of freedom	Comments
J	Tangential stiffness	8 node Isoparametric	Virtual crack extension	0.5	52	418	
K	Tangential stiffness	3 node Constant strain triangle	Path integral (Mean value)	0.1, 0.15	232	278	Displacement formulation
				0.5	320	364	
L	Initial stiffness	8 node Isoparametric	Virtual crack extension	0.5	60	390	
M	Tangential stiffness	3 node Constant strain Δ	Path integral (Mean value)	0.5	300	354	
N	Tangential stiffness	8 node Isoparametric	Path integral (Mean value)	0.5	52	366	
O	Initial stiffness	8 node Isoparametric	J_{es} and Path integral (Mean value)	0.1	103	704	Displacement formulation
				0.15, 0.5	56	394	Applied displacement loading

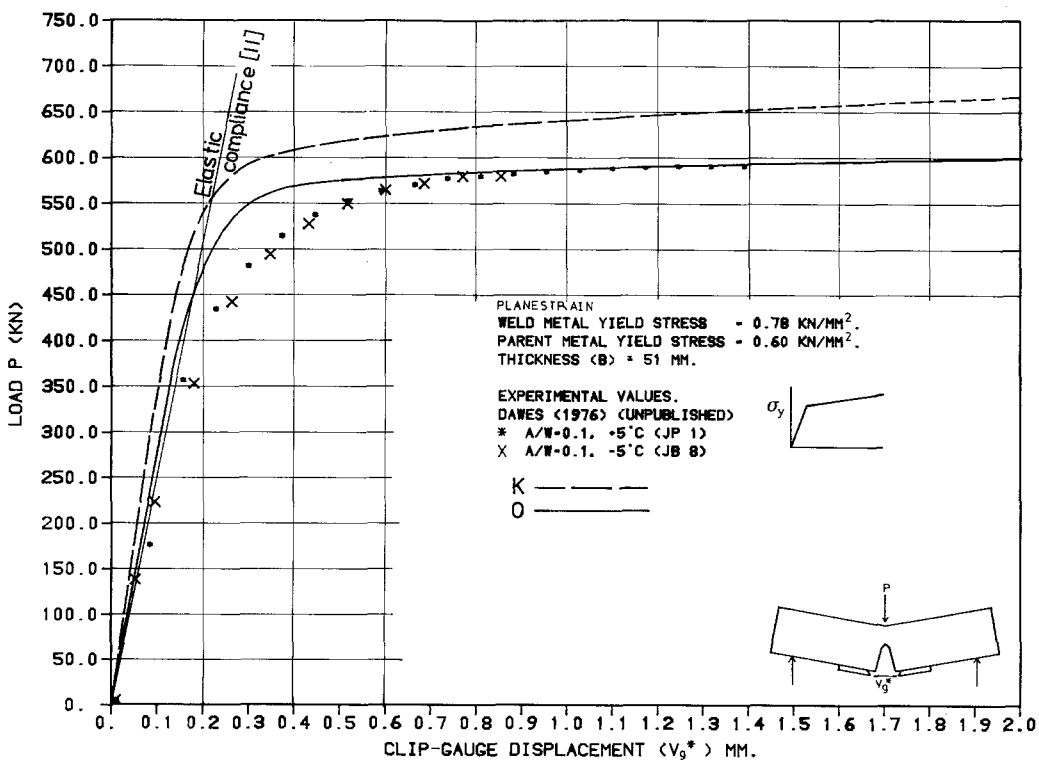

Figure 10a. *Round robin.* Variation of load with clip gauge displacement (V_g^*) for the 3 point BEND weld specimen ($a/w = 0.1$).

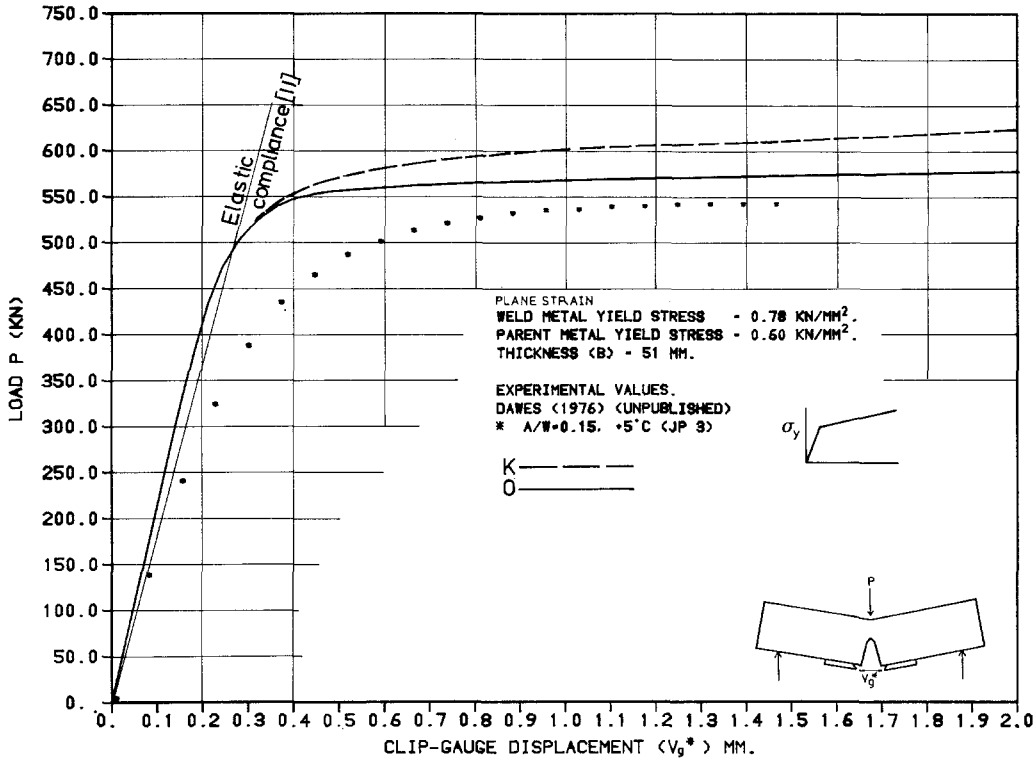

Figure 10b. *Round robin.* Variation of load with clip gauge displacement (V_g^*) for the 3 point BEND weld specimen ($a/w = 0.15$).

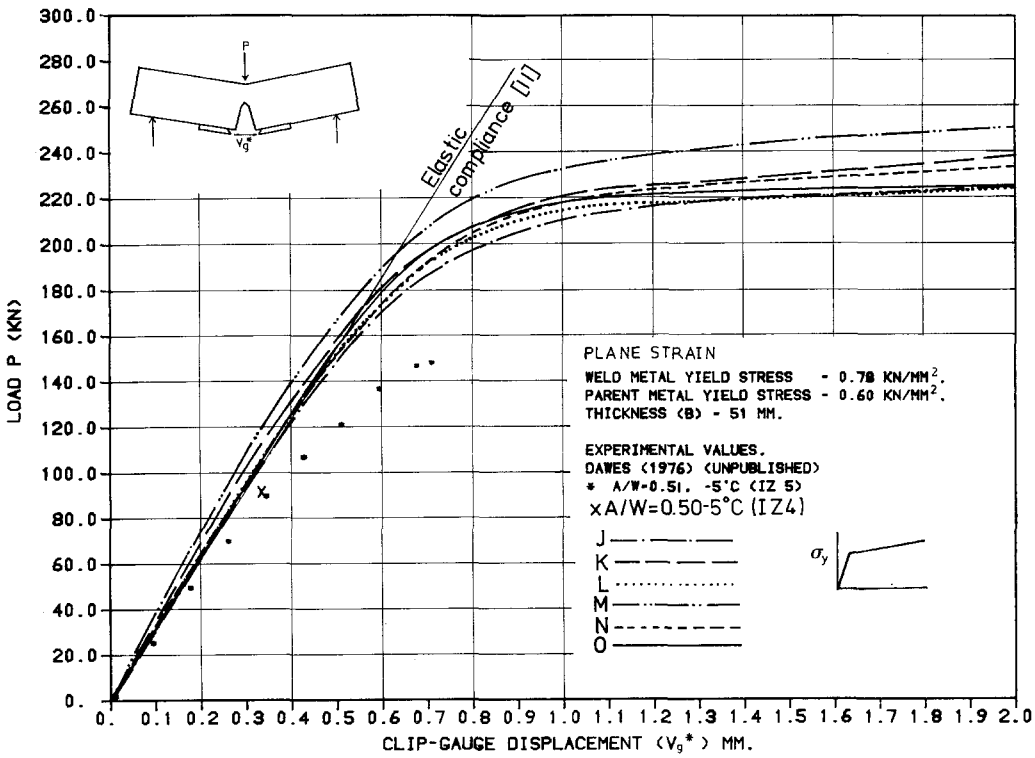

Figure 10c. *Round robin.* Variation of load with clip gauge displacement (V_g^*) for the 3 point BEND weld specimen ($a/w = 0.5$).

and 0.50 respectively. The numerical and known plane strain elastic compliances (obtained by boundary collocation [11]) for each crack length, though in modest agreement with each other, are not in agreement with the experimental compliances. This may be because the specimens cannot be represented by a plane strain constraint and should be represented by a three-dimensional model. The numerical limit loads overestimate the experimental limit loads by a maximum of about 15% in the shallow cracked specimens (Fig. 10a, b). Unfortunately for the standard cracked geometry, the experimental specimen chosen fractured in half before a limit load was achieved. The maximum variation between the numerical results for the standard geometry (Fig. 10c) is about 10%. This is better than that obtained in [1] (for a corresponding $a/W = 0.5$) of approximately 30%.

It is interesting to note that for the standard crack depth, the two contributors using constant strain triangles (K, M) gave the stiffest results in both the linear and non-linear regions, and showed the greatest discrepancies from the elastic compliances (the isoparametric elements all gave good agreement with the elastic compliance). This may be due to the tendency of these triangular elements to give overstiff behaviour in bending problems. However, the difference between these two solutions and the other numerical results is smaller than the discrepancy with the experimental results.

Figures 11a, b, c show $\bar{J}_{co}$ as a function of V_g^* for $a/W = 0.1$, 0.15 and 0.5 respectively. Also shown on these three figures is J_{es} obtained from 1) the experimental load/displacement curve and 2) the numerical load/displacement curve from contributor O.

For $a/W = 0.1$ and 0.15, the two numerical $\bar{J}_{co}$ and numerical J_{es} results are indistinguishable at low displacement levels. At higher levels the discrepancies become more apparent with the two numerical $\bar{J}_{co}$ curves varying by a maximum of 20%. These two numerical $\bar{J}_{co}$

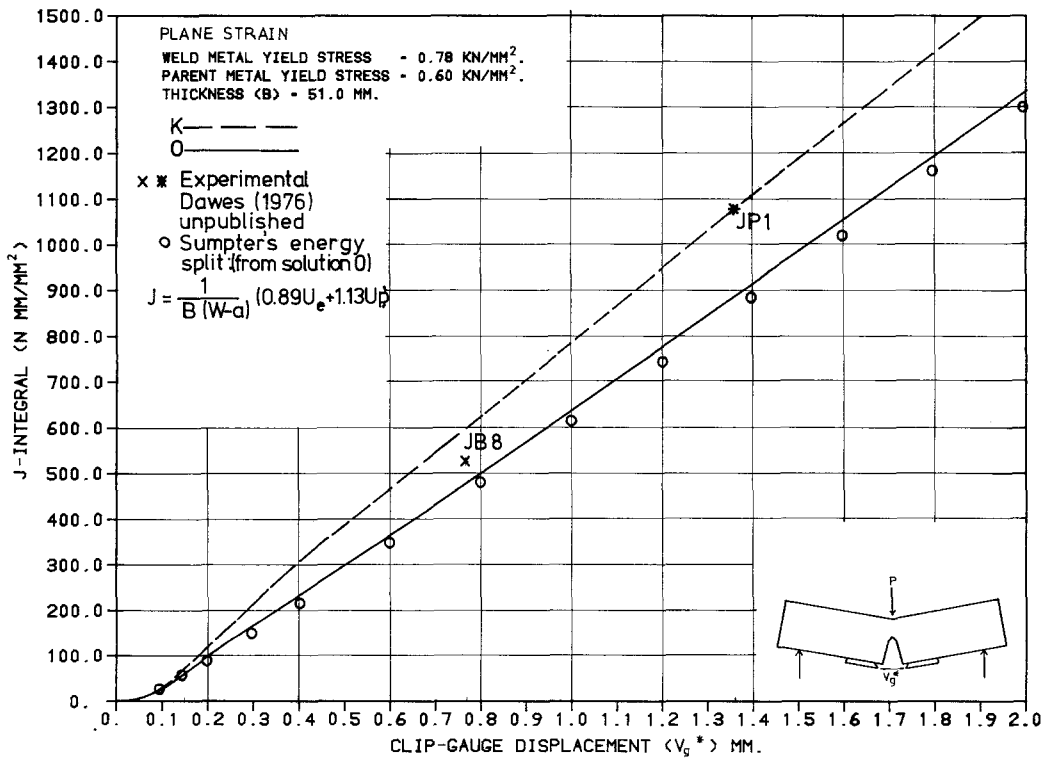

Figure 11a. *Round robin.* Variation of the J integral with clip gauge displacement (V_g^*) for the 3 point BEND weld specimen ($a/w = 0.1$).

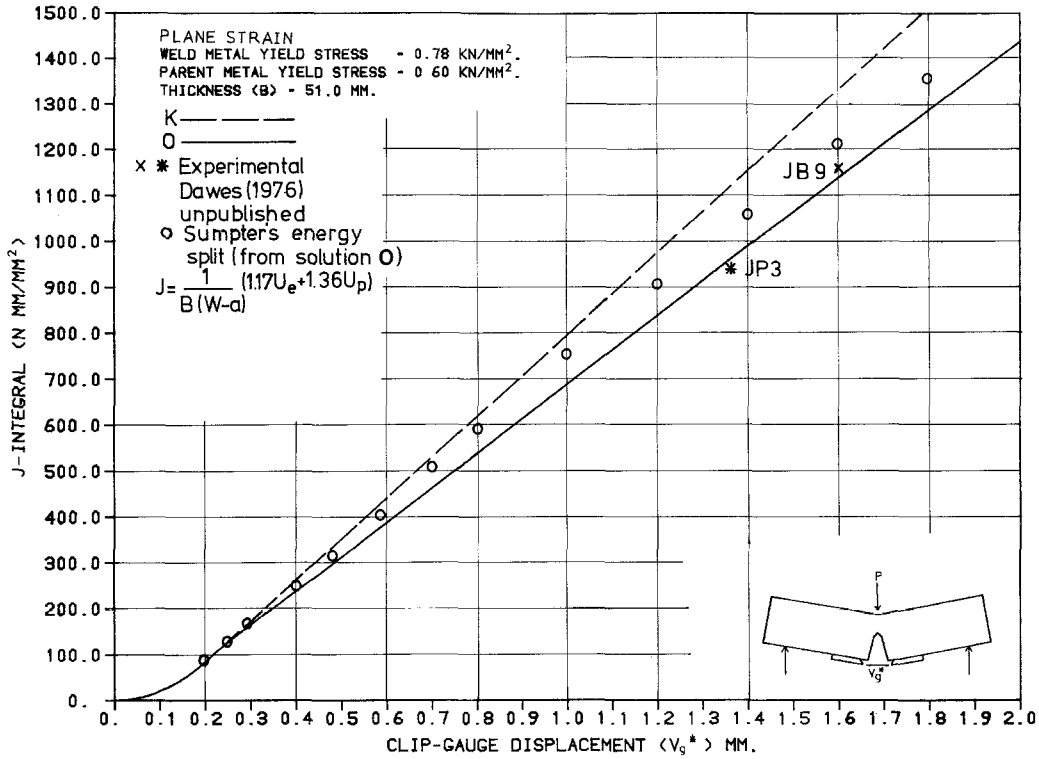

Figure 11b. *Round robin.* Variation of the J integral with clip gauge displacement (V_g^*) for the 3 point BEND weld specimen ($a/w = 0.15$).

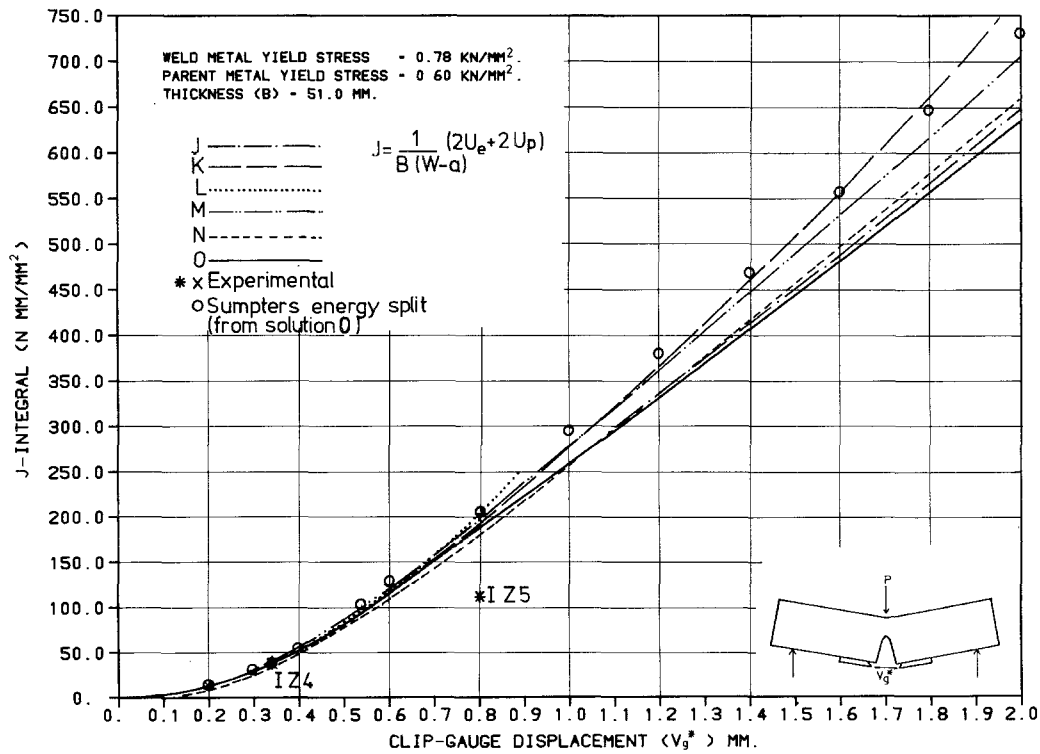

Figure 11c. *Round robin.* Variation of the J integral with clip gauge displacement (V_g^*) for the 3 point BEND weld specimen ($a/w = 0.5$).

curves for each crack length give a rough bound on the numerical and experimental J_{es} results.

All six participants contributed in Fig. 11c for the standard specimen. As mentioned previously, these standard geometries failed in a brittle fashion producing low J values. For the elastic portion of the curve there is good correlation between all the numerical, analytical and experimental results. In the plastic region, the two solutions using constant-strain triangles (K, M) gave significantly higher values, as would be expected from the load/displace-

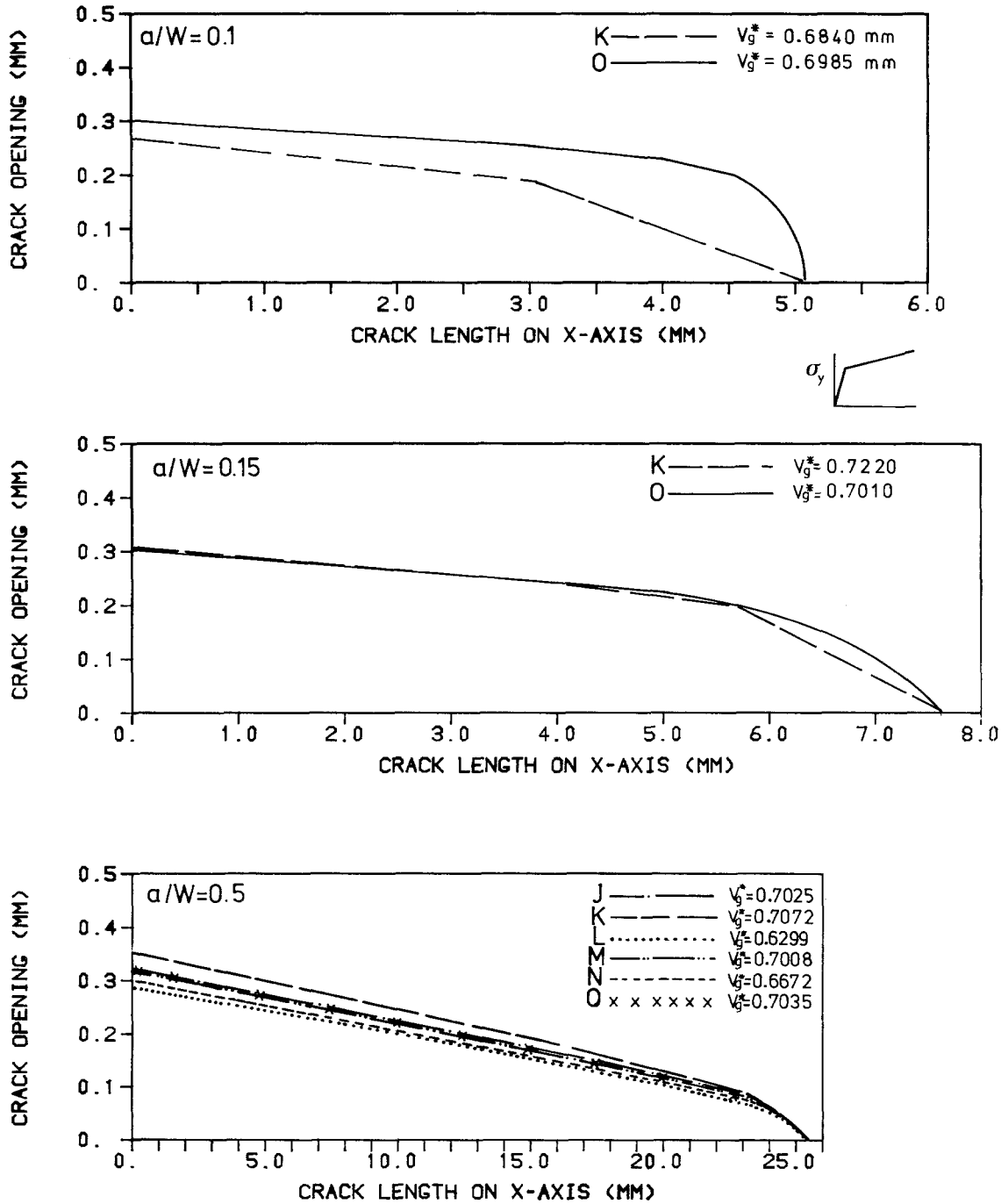

Figure 12. *Round robin.* Semi-crack opening profiles for the 3 point BEND weld specimen at a clip gauge displacement (V_g^*) of approximately 0.7 mm.

ment curves. However, solution L, if extended, would appear to indicate even higher J-values. The maximum deviation between these curves is approximately 15% compared with 29% for the difference between the J/load-point displacement values of [1] at the same load-point displacement.

The crack surface contours for the three crack lengths are shown in Fig. 12 at a displacement of $V_g^* = 0.7$ mm. These profiles seem to be relatively insensitive to the modelling chosen. The only large variation is between solution K and O for $a/W = 0.1$, but this is due to contribution K using constant-strain triangles which fail to show the characteristic COD.

The rotation factors for $a/W = 0.1, 0.15$ and 0.5 are shown in Figs. 13a, b, c, respectively. Slip line theory dictates that once general yield occurs and a hinge forms, the center of rotation r remains constant. The numerical solutions for the two shallow crack geometries are in considerable disagreement. At high loads solution K is actually declining whilst solution O is still rising. The agreement between the six contributors is better in Fig. 13c for the standard geometry. Haigh and Richards [12] quote a value for $r = 0.46$, though in this case the curves are still rising and it may be that the specimens are not loaded sufficiently to attain this value.

Figure 14 shows the plastic zone development for the standard geometry at a value of V_g^* equal to 0.7 mm. Although the meshes vary widely as regards refinement and element type, the plastic zones are very similar from the five contributors (J, L, M, N, O).

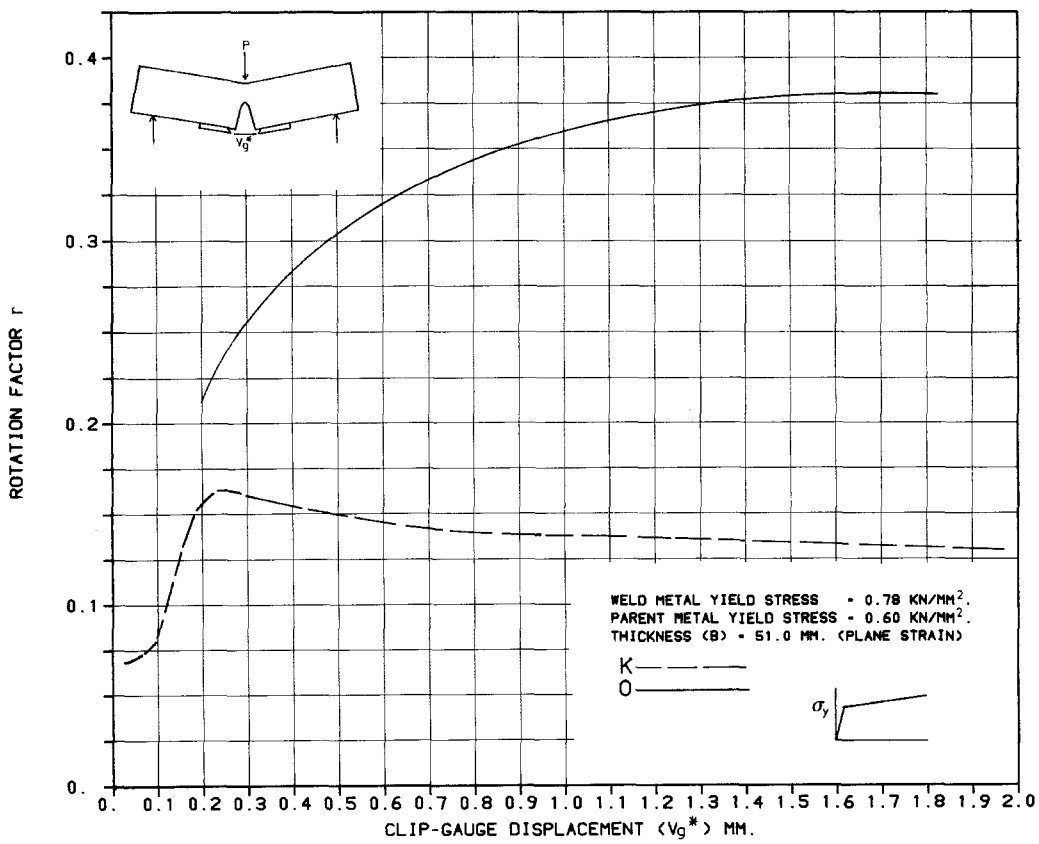

Figure 13a. *Round robin.* Variation of rotation factor with clip gauge displacement (V_g^*) for the 3 point BEND specimen ($a/w = 0.1$).

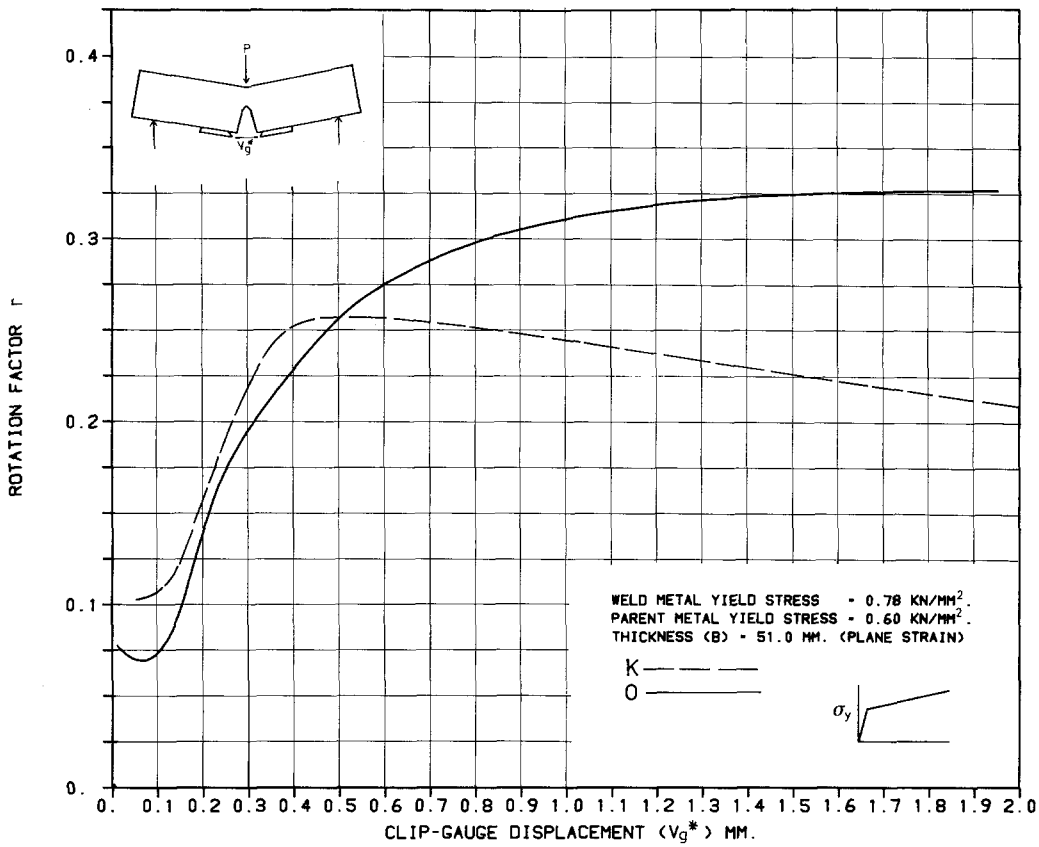

Figure 13b. *Round robin.* Variation of rotation factor with clip gauge displacement (V_g^*) for the 3 point BEND specimen ($a/w = 0.15$).

3.3. K_I *results for the* BEND3 *and* SENT *geometries*

There were five participants (P–T) for this problem with four of them participating in the shallow notch analysis (Table 8a) and all five participating in the standard specimen analysis (Table 8b), with two solutions from P.

Two participants used $\bar{J}_{co}$ and another J_{pe} to determine K_I, using the relationship: $K_I = \sqrt{[EJ/(1-\nu^2)]}$ with E equal to 170.0 kN/mm^2 in the case of the specimens modelled with a weld. The remaining two participants used virtual crack extension [5] and direct displacement [13] formulations. All the solutions for the SENT geometries were modelled using applied displacements.

Participants P–S utilized the eight-noded isoparametric element and T, the constant-strain triangle element. For P, Q, R the midside node of the crack tip element was moved to the quarter-point to represent the $1/\sqrt{r}$ singularity [9] along the edges of the element from the crack tip.

The results obtained from the BEND3 and SENT geometries are listed in Tables 8a and 8b for $a/W = 0.1$ and 0.5, respectively. There are no known theoretical or analytical elastic solutions for the non-homogeneous specimens. Known elastic solutions for the homogeneous BEND3 specimens with $S/W = 4.0$ for $K_I\sqrt{WB}/P = 3.54$ (interpolated value) and 10.61 for the shallow and standard geometries respectively [11]. The corresponding numerical results

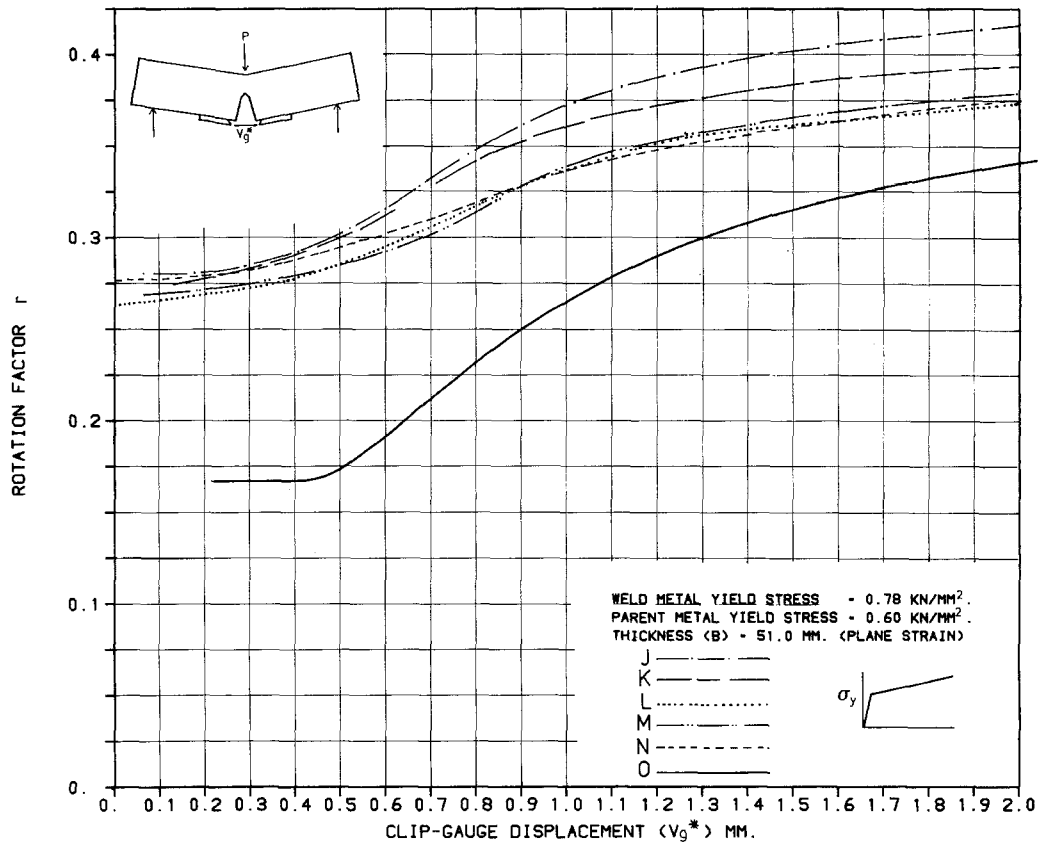

Figure 13c. *Round robin.* Variation of rotation factor with clip gauge displacement (V_g^*) for the 3 point BEND specimen ($a/w = 0.5$).

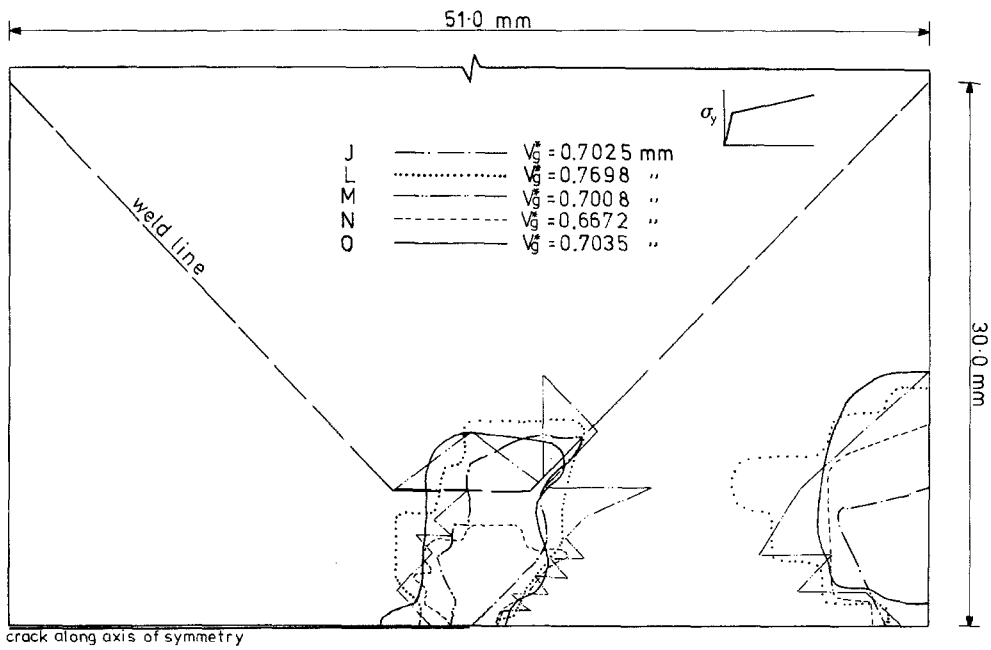

Figure 14. *Round robin.* Plastic zone development for the 3 point BEND weld specimen at a clip gauge displacement (V_g^*) of approximately 0.7 mm ($a/w = 0.50$).

TABLE 8a

Non-dimensional stress intensity factor F_I for the 3 point bend and SENT *elastic round robin problem* ($a/W = 0.1$)

Solution	Element type	Number of elements	Number of degrees of freedom	Computer type	Calculation method of K_I	$\frac{E_w^*}{E_p}$	3 PT. BEND			SENT		
							F_I	CPU Time	Cost** $	F_I	CPU Time	Cost** $
Q	8 node Isoparametric (1/4 point)	90	618	HITAC 8700/8800	Path integral (Mean of 9 paths)	$\frac{210}{210}$	3.20	45.8	1.23	0.646	45.8	1.23
						$\frac{170}{210}$	3.12	45.8	1.23	0.596	45.8	1.23
R	8 node Isoparametric (1/4 point)	90	618	HITAC 8700/8800	Direct displacement	$\frac{210}{210}$	3.04	29.9	0.81	0.600	29.9	0.81
						$\frac{170}{210}$	2.96	29.9	0.81	0.522	29.9	0.81
S	8 node Isoparametric	100	682	CDC 7600	Path integral (Mean of 8 paths)	$\frac{210.0}{210.0}$	3.21	6.8	6.04	0.642	6.72	5.97
						$\frac{170.0}{210.0}$	3.13	6.8	6.04	0.602	6.72	5.97
T	3 node Constant strain	326	371	1906S	Potential energy release	$\frac{210}{210}$	3.17	?	?	0.656	?	?
	Δ				rate	$\frac{170}{210}$	3.11	?	?	0.617	?	?
Rooke and Cartwright [14]						$\frac{210}{210}$	3.25					

$F_I = K_I B\sqrt{W}/P$

* $\frac{E_w}{E_p} = \frac{\text{Young's modules of weld material (kN/mm}^2\text{)}}{\text{Young's modules of parent material (kN/mm}^2\text{)}}$

** University rate

TABLE 8b
Non-dimensional stress intensity factor F_1 for the 3 point bend and SENT *elastic round robin problem* ($a/W = 0.5$)

Solution	Element type	Number of elements	Number of degrees of freedom	Computer type	Calculation method of K_1	$\frac{E_w^*}{E_p}$	3 PT. BEND			SENT		
							F_1	CPU Time	Cost** $	F_1	CPU Time	Cost** $
P	8 node Isoparametric	60	614	CDC 6600 CYBER 74,73	Virtual crack extension	$\frac{210}{210}$	10.02	27.0	14.04	2.08	24.0	12.48
						$\frac{170}{210}$	10.10	27.0	14.04	2.03	24.0	12.48
P	8 node Isoparametric (1/4 point)	60	640	CDC 6600 CYBER 74,73	Virtual crack extension	$\frac{210}{210}$	10.23	27.0	14.04	2.12	24.0	12.48
						$\frac{170}{210}$	10.32	27.0	14.04	2.06	24.0	12.48
Q	8 node Isoparametric (1/4 point)	90	618	HITAC 8700/8800	Path integral (Mean of 4 paths)	$\frac{210}{210}$	10.31	45.8	1.23**	2.11	45.8	1.23**
						$\frac{170}{210}$	10.15	45.8	1.23**	2.01	45.8	1.23**
R	8 node Isoparametric (1/4 point)	90	618	HITAC 8700/8800	Direct displacement	$\frac{210}{210}$	10.15	29.9	0.81**	2.06	29.9	0.81**
						$\frac{170}{210}$	10.02	29.9	0.81**	1.94	29.9	0.81**
S	8 node Isoparametric	54	378	CDC 7600	Path integral (Mean of 4 paths)	$\frac{210}{210}$	9.98	2.87	2.56	2.09	2.913	2.59**
						$\frac{170}{210}$	9.82	2.87	2.56	1.95	2.913	2.59**
T	3 node Constant strain Δ	326	371	1906S	Potential energy release	$\frac{210}{210}$	10.12	?	?	3.47	?	?
						$\frac{170}{210}$	10.03	?	?	3.40	?	?
Rooke and Cartwright [14]						$\frac{210}{210}$	10.41					

$F_1 = K_1 B\sqrt{W}/P$ * $\frac{E_w}{E_p} = \frac{\text{Young's modules of weld material (kN/mm}^2)}{\text{Young's modules of parent material (kN/mm}^2)}$ ** University rate

all underestimate these values by a maximum of 14.1 and 5.9%, respectively. This latter value compares with 4% from [1]. A difficulty arises with the homogeneous SENT specimens, for although accurate elastic solutions exist for the geometries with bending unrestrained [14], this is not the case with restrained bending, which occurs with uniform applied displacements.

The costs of analysis varied widely, with the standard notch analysis showing much greater variation. However, solution P (Table 8b) for the standard notch is based on commercial rates and the rest on university rates.

3.4. *Center-cracked panel* (CCP) *results*

Three contributions (U–W) were obtained for the CCP analysis. Two of the contributors employed the tangential stiffness method and the third initial stiffness (Table 9).

Due to symmetry only one-quarter of the specimen was analyzed with the crack aligned along an axis of symmetry, so that slow crack growth could be modelled by releasing the restrained nodes along the boundary. Two of the solutions used the eight-noded isoparametric element whilst the third used various isoparametric elements varying from four to eight nodes.

A two-dimensional analysis cannot model the 45 degree slant nature of the actual fracture surface, and all contributors assumed that "flat fracture" occurred.

Although it was intended that a fracture criterion should be utilized to model the slow crack growth, solutions U and V used the relationship between crack extension and clip gauge displacement (detailed in Fig. 7) to obtain the required load/displacement curve. Solution W used a single valued parameter Q [15] equal to the work done in releasing the nodal reactions ahead of the crack-tip in order to advance the crack. After the first extension (decided by inspection of the experimental data) a critical value Q_c was calculated and subsequent crack extension was allowed according to the condition $Q > Q_c$.

The numerical and experimental load/clip gauge displacement curves are shown in Fig. 15. The three numerical solutions show good correlation with each other, but they all overestimate the elastic compliance of the experimental curve. It is only after slow crack growth has occurred, that all the curves coincide at a maximum load of approximately 80 kN. Although the experimental and numerical modelling was done under displacement control, only solution V shows a drop in load as slow crack growth proceeds, because the other curves have been "smoothed".

TABLE 9
Basic details round robin problem of the centre notch

Solution	Plasticity method	Element type	Number of elements in quarter space mesh	Number of degrees of freedom
U	Tangential stiffness	8 node Isoparametric	35	268
V	Tangential stiffness	4–8 noded Isoparametric	50	272
W	Initial stiffness	8 noded Isoparametric	52	185

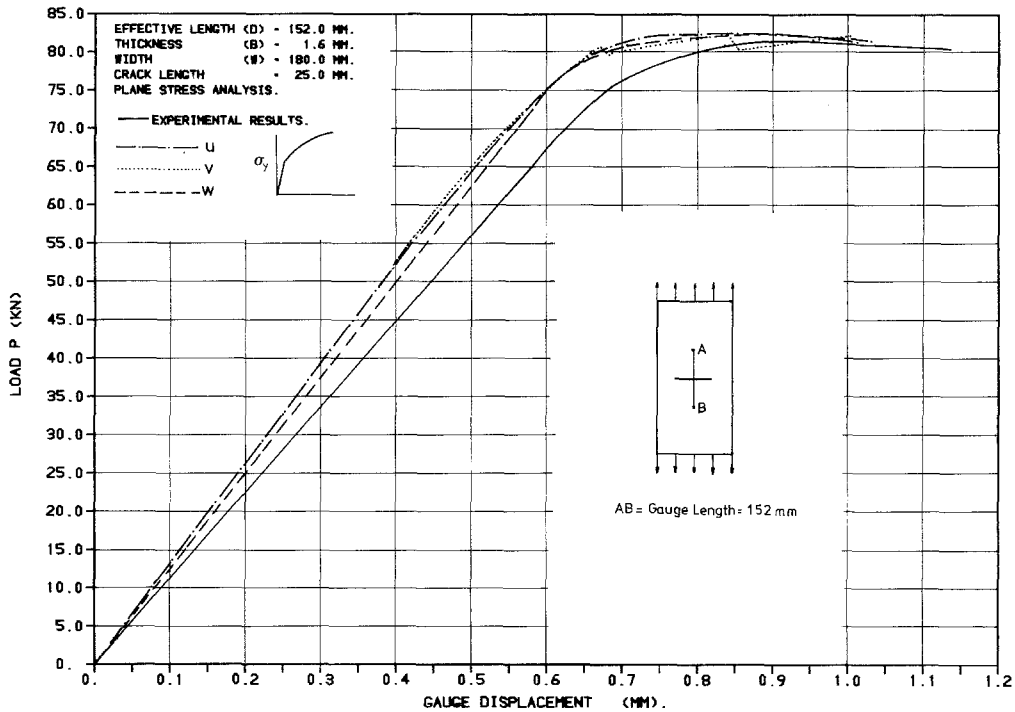

Figure 15. *Round robin.* Variation of load with gauge displacement for the centre notch propagating aluminium specimen.

4. Conclusions

This elastic-plastic round robin has been concerned with three types of geometry and in general the correlation of results has been good, particularly for the numerical load/displacement curves.

With the exception of two contributions to the J/V_g results (reasons are given for these contributors' discrepancies), there is very good agreement between the numerical and experimental $P, J/V_g$ curves for the CS analysis. These results show less deviation than those of [10], for their "non-standard" problem but not for their "standard" problem where discrepancies occur only at high load levels.

The numerical solutions for the three-point geometry show a greater scatter than those from the compact specimen, but this scatter is smaller than that demonstrated in the paper by Wilson and Osias [1].

The fact that the numerical variation for the BEND3 is greater than that for the CS geometries may be due to the concentrated load on the axis of symmetry, adjacent to the crack. Reliable numerical modelling of concentrated loads in elastic-plastic stress fields requires more detailed information than that provided in the current study. Deviation of the BEND3 numerical results from the experimental data may be indicative of some three-dimensional effects in the real situation.

As with the BEND3 analysis, the numerical P/V_g results for the CCP specimen modelling slow crack growth, although in good agreement with each other, overestimate the experimental compliances. It is only at the maximum load that there is agreement between the numerical and experimental results for the CCP specimen.

REFERENCES

[1] W.K. Wilson and J.R. Osias, *International Journal of Fracture* 14 (1978) R98–R109.
[2] J.G. Merkle and H.T. Corten, *Journal of Pressure Vessel Technology* 96 (1974) 286–292.
[3] J.R. Rice, *Journal of Applied Mechanics* 35 (1968) 379–386.
[4] J.R. Rice, in *Fracture and Advanced Treatise*, Ed. H. Liebowitz, Volume II (1968) 191–311.
[5] D.M. Parks in *Proceedings of the First International Conference of Numerical Methods in Fracture Mechanics* Swansea University, U.K. (1978) 464–478.
[6] J.D.G. Sumpter and C.E. Turner, in *Cracks and Fracture*, ASTM STP 601 (1976) 3–18.
[7] *Standard Method of Test For Plane Strain Fracture Toughness of Metallic Materials.* ASTM E-74 (1974).
[8] F.J. Bradshaw and C. Wheeler, "The Crack Resistance of Some Aluminium Alloys and the Prediction of Thin Section Failure", Report 73191, Royal Aircraft Establishment, Farnbourgh, England (1974).
[9] R.S. Barsoum, *International Journal for Numerical Methods in Engineering* 10 (1976) 25–37.
[10] M. Shiratori and T. Miyoshi, in *Proceedings of the Second International Conference of Numerical Methods in Fracture Mechanics* Pineridge Press, Swansea, U.K. (1980) 417–431.
[11] J.E. Srawley and B. Gross, *Engineering Fracture Mechanics* 4 (1972) 587–589.
[12] J.R. Haigh and C.E. Richards, Report RD/L/M 461, Central Electricity Generating Board, U.K. (1974).
[13] G. Irwin, *Journal of Applied Mechanics* 24 (1957) 361–364.
[14] D.P. Rooke and D.J. Cartwright, in *Compendium of Stress Intensity Factors* (1976) 84.
[15] W.T. Evans, M.F. Light and A.R. Luxmoore, *Journal of the Mechanics and Physics of Solids* 28 (1980) 167–189.

RÉSUMÉ

Les résultats d'éléments finis non linéaires résultant d'une consultation circulaire sont comparés avec des données empiriques et expérimentales obtenues pour trois types de géométrie: éprouvette compacte, éprouvette de flexion en trois points et panneau à fissure centrale soumis à une charge uniaxiale. Les paramètres de la solution qui doivent être comparés dans les différentes formes sont: la charge appliquée, le déplacement d'un extensiomètre, l'intégrale J (sans réserve sur sa méthode de calcul), KI, les profils d'ouverture de fissure ainsi que le développement de la zone plastique.